UC Riverside
2016 Publications

Title
Novel Approach for Evaluating Secondary Organic Aerosol from Aromatic Hydrocarbons: Unified Method for Predicting Aerosol Composition and Formation

Permalink
https://escholarship.org/uc/item/5dh9v1z5

Journal
Environmental Science & Technology, 50(12)

ISSN
0013-936X 1520-5851

Authors
Li, Lijie
Tang, Ping
Nakao, Shunsuke
et al.

Publication Date
2016-06-21

DOI
10.1021/acs.est.5b05778

Peer reviewed

Novel Approach for Evaluating Secondary Organic Aerosol from Aromatic Hydrocarbons: Unified Method for Predicting Aerosol Composition and Formation

Lijie Li,[†,‡] Ping Tang,[†,‡] Shunsuke Nakao,[†,‡] Mary Kacarab,[†,‡] and David R. Cocker, III*[,†,‡]

[†]Department of Chemical and Environmental Engineering, University of California, Riverside, Riverside, California 92521, United States

[‡]College of Engineering, Center for Environmental Research and Technology (CE-CERT), University of California, Riverside, Riverside, California 92507, United States

Ⓢ Supporting Information

ABSTRACT: Innovative secondary organic aerosol (SOA) composition analysis methods normalizing aerosol yield and chemical composition on an aromatic ring basis are developed and utilized to explore aerosol formation from oxidation of aromatic hydrocarbons. SOA yield and chemical composition are revisited using 15 years of University of California, Riverside/CE-CERT environmental chamber data on 17 aromatic hydrocarbons with HC:NO ranging from 11.1 to 171 ppbC:ppb. SOA yield is redefined in this work by normalizing the molecular weight of all aromatic precursors to the molecular weight of the aromatic ring

$$\text{Yield}' = \text{Yield}_i \times \frac{MW_i}{MW_{\text{Aromatic ring}}},$$ where i is the aromatic hydrocarbon

precursor. The yield normalization process demonstrates that the amount of aromatic rings present is a more significant driver of aerosol formation

than the vapor pressure of the precursor aromatic. Yield normalization also provided a basis to evaluate isomer impacts on SOA formation. Further, SOA elemental composition is explored relative to the aromatic ring rather than on a classical mole basis. Generally, four oxygens per aromatic ring are observed in SOA, regardless of the alkyl substitutes attached to the ring. Besides the observed SOA oxygen to ring ratio (O/R ~ 4), a hydrogen to ring ratio (H/R) of $6 + 2n$ is observed, where n is the number of nonaromatic carbons. Normalization of yield and composition to the aromatic ring clearly demonstrates the greater significance of aromatic ring carbons compared with alkyl carbon substituents in determining SOA formation and composition.
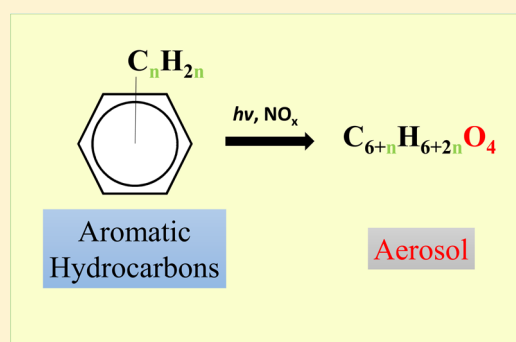
1. INTRODUCTION

Challenges remain in predicting anthropogenic secondary organic aerosol (SOA) with anthropogenic SOA sources underestimated in current models by a factor of up to 10.[1−9] It is imperative to develop SOA predictive frameworks in order to help models predict SOA formation from a wide variety of aerosol precursors given limited experimental resources. Aromatic hydrocarbons are an example of a major class of anthropogenic SOA precursors[6,10−12] that can benefit from such a predictive framework as their SOA formation is explored for increasingly relevant atmospheric conditions.

Importing reasonable SOA formation parameters into models is essential for accurate estimates of global and regional SOA budgets. SOA yield is a function of the extent of gas-to-particle conversion, which depends on the vapor pressure of the absorbing species.[13] Recent studies also demonstrate the importance of aqueous chemistry[14] and heterogenous reaction.[15] However, collecting reliable SOA parameters for every aerosol precursor requires significant effort and time. Therefore, a general rule to predict SOA yield and chemical composition by precursor category is valuable for SOA prediction.

Traditionally, two-product models simulate SOA yield by categorizing all oxidation products into two lumped semi-volatile products according to their gas-particle phase partitioning coefficient.[13,16] The volatility basis set (VBS) stems from the two-product model by assigning volatile organic compound (VOC) oxidation products to volatility "bins", which span across multiple ambient organic effective saturation mass concentrations (C^*).[17] Several models have also been established based on the two-product and/or VBS model by adding tunable parameters that estimate chemical polarity, polymerization, fragmentation, functionalization, and elemental ratio.[18−21] More complicated models are also developed considering explicit gas and particle phase reaction mechanisms[22−24] and phase state impact.[5,25,26] Newly developed models are calibrated and tuned with alkanes[21,24] and biogenic SOA precursors.[19,20] Ensuring the accuracy of SOA prediction

from aromatic hydrocarbon photooxidation under ambient conditions improves the SOA prediction in current models.[27] Due to the limited understanding of aromatic oxidation chemistry, the applicability of these models to a variety of aromatic hydrocarbons requires further work.

Earlier two-product model fittings to aromatic hydrocarbon oxidation are not applicable to ambient atmospheric conditions,[28,29] as they were conducted at NO_x concentrations that are not atmospherically relevant (>100 to 1000 ppb). Recent studies on the photooxidation of aromatic hydrocarbons at lower NO_x levels only focus on a few selected aromatic precursors.[30−32] Therefore, a new systematic study on SOA formation as a function of aromatic molecular structure is required at more relevant atmospheric conditions to elucidate how these compounds are truly behaving in the atmosphere. Odum's work summarizes the SOA yields formed from the oxidation of aromatics into two groups (low yield and high yield group).[28] This work improves upon this earlier work by providing SOA yields at more realistic conditions (e.g., NO_x concentration simulating urban regions) with tighter controls on the environmental conditions (e.g., temperature and light intensity). Our earlier work[33] found that traditional mass-based SOA yields for aromatic hydrocarbons are associated with the number of alkyl substitutes in the aromatic precursor. Further studies are still needed to explore the underlying mechanisms leading to the relationship in between SOA formation and aromatic hydrocarbon molecular structure.

Elemental analysis[34,35] can help elucidate SOA chemical composition and formation mechanisms.[36,37] Previous SOA product studies observed a decrease in oxygen to ring ratio (O/C) and an increase in hydrogen to ring ratio (H/C) with the addition of alkyl substitutes attached to the precursor aromatic ring,[37−39] resulting in a lower measured oxidation state of carbon (OSc)[40] with an increasing number of alkyl substitutes. However, the low H/C ratio or high degree of unsaturation (double bond equivalent = 4) of the aromatic ring makes the H/C of aromatic hydrocarbons more dependent on the number of substituted alkyl carbons than more saturated precursors. This dependence of H/C on alkyl carbon substitutes is likely retained in aromatic SOA products. Further, the carbon on the aromatic ring may behave differently than the alkyl substitute carbon with respect to overall O/C. Therefore, evaluating the extent of aromatic hydrocarbon oxidation solely relying on average SOA H/C and O/C without distinguishing between alkyl substitute and aromatic ring carbons may conceal the compositional similarity among SOA from different aromatics. Refinement of the SOA elemental ratio interpretation is required to clarify the contribution of different functional groups to the SOA formation from aromatic hydrocarbons.

The motivation of this study is to improve the understanding of aromatic hydrocarbon SOA formation using innovative methods developed within this study. SOA yield and chemical composition are reanalyzed on the basis of the aromatic ring using 15 years of University of California, Riverside (UC Riverside)/CE-CERT chamber data on 17 aromatic hydrocarbons with HC:NO ratio ranging from 11.1 ppbC:ppb to 171 ppbC:ppb. Specific and general alkyl substitute or molecular structure impacts to SOA formation from single ring aromatic hydrocarbons are explored.

2. METHODS

All experiments (Table S1) were conducted in the UC Riverside/CE-CERT indoor dual 90 m³ environmental

chambers.[41] Experiments were conducted at dry conditions (RH < 0.1%) in the absence of inorganic seed aerosol and with temperature controlled to 27 ± 1 °C. Particle size distribution between 27 and 686 nm was monitored by dual custom built scanning mobility particle sizers (SMPS).[42] Particle effective density was measured with a Kanomax aerosol particle mass analyzer (APM-SMPS) system.[43] Evolution of particle-phase chemical composition was measured by a high resolution time of flight aerosol mass spectrometer (HR-ToF-AMS; Aerodyne Research, Inc.).[44,45] The Agilent 6890 gas chromatograph−flame ionization detector was used to measure aromatic hydrocarbon concentrations. A Thermal Environmental Instruments Model 42C chemiluminescence NO analyzer was used to monitor NO, NO_y−NO, and NO_y.

A suite of 17 aromatic hydrocarbon (zero to six alkyl substitutes ranging in carbon number from one to three) SOA precursors was studied. Detailed environmental conditions for the 17 aromatic precursors are described previously.[33,46] The reaction activities (e.g., $k_{OH}*[OH]$, $[HO_2]*[RO_2]$) are comparable for all aromatic precursors studies.[33,46] Seeded experiments to minimize wall effects have also been conducted in our chamber experiment with no measurable difference observed between the seeded and nonseeded experiment. This indicates that the gas-phase wall loss might not actually be significant in our chamber for aromatic SOA experiments.

This study defines a ring-normalized SOA yield (Yield′) by adjusting yield from per aromatic precursor mass consumption to per aromatic ring mass assumption to elucidate the SOA formation potential per aromatic ring or per mole instead of the traditional per total mass method. Ring-normalized SOA yield (Yield′) is calculated as

$$\text{Yield}' = \frac{M_0}{(\Delta HC_i / MW_i) \times MW_{AR}} = \frac{M_0}{\Delta HC_i} \times \frac{MW_i}{MW_{AR}}$$
$$= \text{Yield}_i \times \frac{MW_i}{MW_{AR}} \quad (1)$$

where MW_i (g mol⁻¹) is the molecular weight of a specific aromatic hydrocarbon i (g mol⁻¹), and MW_{AR} is the molecular weight of an aromatic ring (78 g mol⁻¹ assuming C_6H_6). Yield_i is the traditional SOA mass yield of each aromatic hydrocarbon (i) precursor defined by Odum et al.[13] as

$$\text{Yield}_i = \frac{M_0}{\Delta HC_i} \quad (2)$$

where M_0 (μg m⁻³) is the particle phase organic mass concentration produced from the amount of aromatic hydrocarbon (i) precursor reacted, ΔHC_i (μg m⁻³).

Elemental ratios[34,35] have been reported using AMS data in many studies.[37−39] Recent work by Li et al.[33] demonstrates that the addition of methyl groups to the aromatic ring reduces the average oxidation extent of carbon in SOA formed from aromatic hydrocarbons. The current work redefines elemental ratio on an aromatic ring basis (eqs 3 and 4) to examine the oxygen and hydrogen content in SOA on a per aromatic ring basis. Therefore, we define O/R and H/R as the oxygen and hydrogen content per aromatic ring, calculated as follows:

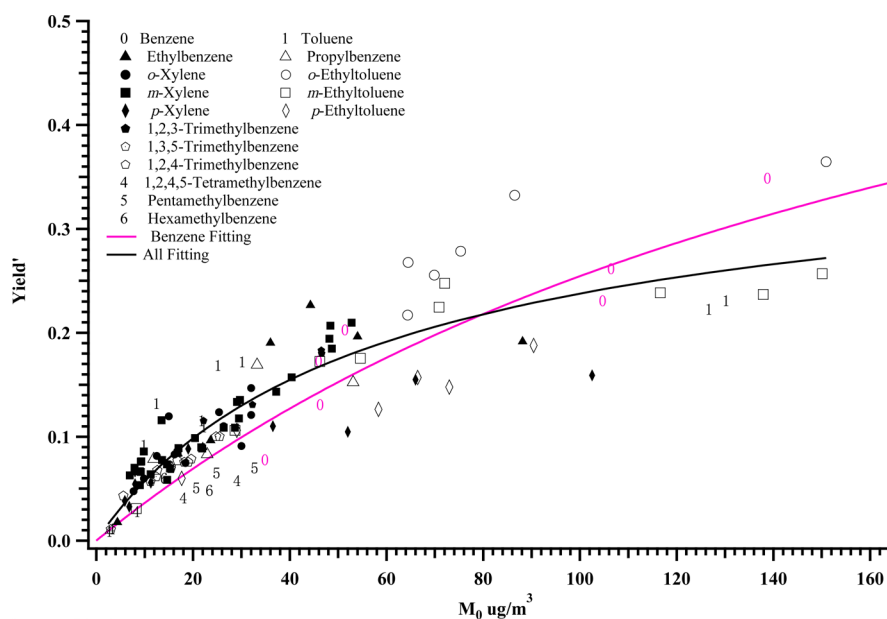$$O/R = C/R_i \times O/C \quad (3)$$

$$H/R = C/R_i \times H/C \quad (4)$$

Figure 1. Molecular weight adjusted SOA Yield (Yield′) as a function of mass loading (M_0 μg/m^3). Each marker or number stands for one or two (hollow triangle stands for *n*-propylbenzene and isopropylbenzene) aromatic hydrocarbons as listed in the graph legend. Numbers stand for aromatic hydrocarbon without isomers studied: 0, benzene; 1, toluene; 4, 1,2,4,5-tetramethylbenzene; 5, pentamethylbenzene; 6, hexamethylbenzene. Pink curve: Two-product model benzene curve fitting. Black curve: Molecular weight adjusted SOA Yield two-product model curve fitting for 17 aromatic hydrocarbons.

where C/R_i represents carbon number on aromatic hydrocarbon i and H/C and O/C are the traditional mole based elemental ratios.[34,35]

3. RESULTS

3.1. Ring-Normalized SOA Yield (Yield′). The physical meaning of ring-normalized SOA yield (Yield′) is SOA formation per mass of aromatic ring consumed. Yield′ technically compares SOA yield from aromatic hydrocarbons on a mole basis since the mass of aromatic ring consumed is proportional to the mole of aromatic hydrocarbon consumed. It is reported that SOA yields from aromatic hydrocarbons decrease with an increase of the number of methyl groups.[33] The ring-normalized SOA yield (Yield′) scales up the low SOA yield by using the ratio of the molecular weight of aromatic precursor and benzene, which is larger than 1, and improves the SOA yield similarity among all aromatic precursors. Ring-normalized SOA Yield (Yield′) as well as traditional mass-based SOA yield are listed in Table S2. Yield′ and M_0 relationships are plotted (Figure 1) similarly to the traditional SOA yield curve in Odum's work.[13] The benzene yield fitting curve in Figure 1 (pink curve) is the same as Figure S1 and is provided as a reference Yield curve. Yield′ from all aromatic hydrocarbons cluster around the fitted curve of benzene (pink curve, Figure 1) instead of scattering to lower yield curves, traditionally used to describe aromatic SOA formation (Figure S1).[33,46] The improvement from scattering to gathering in SOA yield suggests that a similar amount of SOA is formed during the photooxidaiton of each aromatic hydrocarbon when similar amount of aromatic ring involved in the reaction. Similarity of the ring-normalized SOA yield among all aromatic hydrocarbons reveals that the aromatic ring contributes more to SOA formation than the alkyl substitute. A semiempirical two-product model fit approach similar to Odum et al.[13] is used to fit the Yield′ versus M_0 data in this work to further demonstrate the similarity among all SOA yield′ for aromatic hydrocarbons.

The overall two-product model fitting parameters (α_1', $K_{om,1}'$, α_2', and $K_{om,2}'$, Table 1) were determined by minimizing the sum of the square of the residuals.

Table 1. Two-Product Yield Curve Fitting Parameters for Ring-Normalized SOA Yield (Yield′) vs M_0 (μg m^{-3}) in All Ortho (AO), All_meta_TMB_1S (AMT1), All Para_C$_{10+}$ (AP10), and Benzene

Yield′ Curve	α_1'	$K_{om,1}'$ (m^3 μg^{-1})	α_2'	$K_{om,2}'$ (m^3 μg^{-1})
All	**0.310**	**0.021**	**0.086**	**0.005**
AO	0.120	0.022	0.685	0.005
AMT1	0.300	0.021	0.077	0.005
AP10	0.280	0.017	0.030	0.005
benzene[a]	0.082	0.017	0.617	0.005

[a]Note: $\alpha_1 = \alpha_1' = 0.082$; $K_{om,1} = K_{om,1}' = 0.017$; $\alpha_2 = \alpha_2' = 0.617$; $K_{om,2} = K_{om,2}' = 0.005$.[33]

The 17 aromatic hydrocarbons studied (consisting of 129 data points) are fit with a single curve with a mean squared relative error (MSRE) of 13.7×10^{-2} (Table S3), nearly half of the MSRE (24.6×10^{-2}) of the single curve fit performed using traditional yield and M_0. The difference (Figure 1) between the benzene fitted curve (pink) and the overall yield′ fitted curve (dark) indicates a lower yield in benzene at lower mass loading (<50 μg/m^3) and a higher yield at higher mass loading (>100 μg/m^3) than the ring-normalized SOA yield (Yield′). Overall, the application of ring-normalized SOA yield reveal that SOA formation from aromatic hydrocarbons are dependent on the mole of aromatic ring reacted rather than the mass of whole aromatic molecular mass consumed during the photooxidation.

3.2. Aromatic Ring-Based SOA Elemental Ratio. O/R and H/R calculate SOA chemical composition on a precursor aromatic ring basis. They are derived from O/C and H/C and advances O/C and H/C by integrating the impact of the precursor molecular structure on SOA formation into the bulk

chemical composition analysis. An average O/R = 4.08 ± 0.26 (standard deviation equally weights O/R for each group of aromatic hydrocarbons with similar total number of carbon) is observed for SOA originating from the 17 aromatic hydrocarbons studied in this work (Figure 2). The similarity of O/R
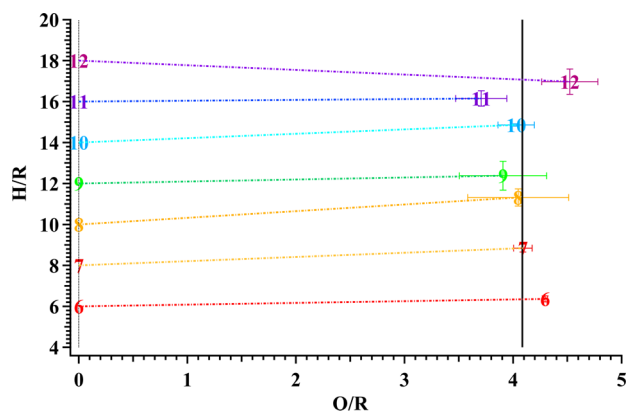

Figure 2. Aromatic ring-based elemental ratios (H/R vs O/R) from the photooxidation of 17 aromatic hydrocarbons. Left number group represents location of aromatic precursors and dashed line O/R = 0. Right number group represents average location of SOA chemical composition from corresponding aromatic hydrocarbon(s) with same carbon number. Solid line represents the location of average O/R = 4.08: 6, benzene; 7, toluene; 8, ethylbenzene and xylenes (meta, para, and ortho); 9, propylbenzene (n- and iso) and trimethylbenzenes (1,2,4-trimethylbenzene, 1,2,3-trimethylbenzene, and 1,3,5-trimethylbenzene); 10, 1,2,4,5-tetramethylbenzene; 11, pentamethylbenzene; 12, hexamethylbenzene.

from single aromatic ring hydrocarbons with different number of total carbons (6 to 12) indicates that each aromatic precursor gains four oxygen when oxidized to SOA regardless

of alkyl substitution. Observed H/R increases in SOA composition along with increasing H/R of the aromatic precursor, which can be seen by the approximately flat dotted lines connecting the H/R of the aromatic precursors to the average H/R of resulting SOA in Figure 2.

The bulk SOA composition during aromatic photooxidation can be predicted according to alkyl carbon number (n) as

$$C:H:O = (6 + n):(6 + 2n):4 \quad (5)$$

where n is the number of alkyl carbons.

Current work provides a simple and reliable method to explain and further predict SOA composition from aromatic precursors for implementation into SOA models. Equation 5 further implies that the average double bond equivalents of aromatic SOA is 4.

3.3. Influence of Isomers on SOA Yield'. While a single Yield' curve fitting provides a reasonable estimation of Yield' for all aromatic compounds, the estimation for individual aromatics can be further improved by accounting for structural isomer effects. Previous work on isomer trends using mass-based yield (e.g., Li et al.[46]) directly applies to Yield' as isomers have identical molecular weights. Therefore, the overall yield fit can be further refined by using separate curves for ortho-, meta-, and para-isomers (Figure 3). Slightly higher SOA yields observed during aromatic hydrocarbon photooxidation for ortho position isomers and lower SOA yields from para position isomers[46] are persistent in ring-normalized SOA yields. Benzene has a somewhat unique trend likely due to enhanced bicyclic hydroperoxide formation[33] and is therefore given a fourth curve in this refined analysis. Ring-normalized yields between aromatics with similar structure (ortho, meta, para), but differing carbon numbers are observed to collapse onto single curves defined by their structure. Monosubstituted aromatics and trimethylbenzene isomers most closely associate
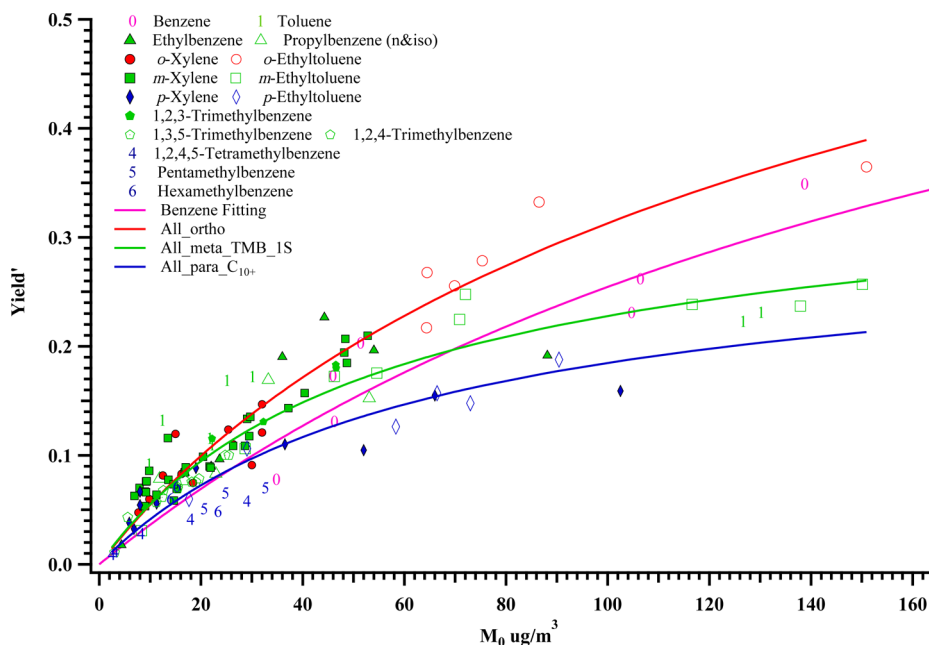

Figure 3. Molecular weight adjusted SOA Yield (Yield') as a function of mass loading (M_0 μg m^{-3}). Each marker or number stands for one or two (hollow green triangle stands for n-propylbenzene and isopropylbenzene) aromatic hydrocarbons as listed in the graph. Number stands for aromatic hydrocarbon without isomers studied: 0, benzene; 1, toluene; 4, 1,2,4,5-tetramethylbenzene; 5, pentamethylbenzene; 6, hexamethylbenzene. Curves are fitted two-product model curves of each isomer group: pink, benzene; red, ortho (AO); green, meta, one substitute and trimethylbenzenes (AMT1); blue, para and those with four more alkyl substitutes (AP10). Marker and number colors are same as their fitting curves.

with the meta-isomer curve and are therefore lumped into the same meta-isomer curve. Aromatics with four or more substituents (C_{10+}) tend to have lower Yield′ falling closest to the para curve. This agrees with the suppression impact of para isomers and C_{10+} aromatic hydrocarbons is proposed in earlier work.[30,43] Therefore, only C_{10+} and two substitute aromatics including para and ortho structure have a small either promotion or suppression effect on SOA formation. AMT1 represents the major SOA formation trend for aromatic hydrocarbons.

The four refined curves (all ortho aromatics, AO; all meta aromatics, mono-substituted aromatics, and trimethylbenzenes, AMT1; all para aromatics and C_{10+} aromatics, AP10; and benzene) are then fit with a modified (Yield′ instead of Y) two-product model ($\alpha_1′$, $\alpha_2′$, $K_{om,1}′$, $K_{om,2}′$; Table 1). A constant $K_{om,2}′$ (more volatile lumped species parameter) is assumed for all curve fits to focus on the yield difference caused by the less volatile ($K_{om,1}′$) products. MSRE for the AMT1 curve decrease from 17.9×10^{-2} to 14.8×10^{-2} when the SOA yield is normalized on a ring basis. Similar MSRE decreases are also observed (Table S3) for the AP10 and AO while applying ring-normalized SOA yield instead of traditional mass-based yield. The benzene curve ($\alpha_1 = 0.082$, $K_{om,1} = 0.017$, $\alpha_2 = 0.617$ and $K_{om,2} = 0.005$)[33] is seen to behave most similarly to the lowest yield group (AP10) at atmospherically relevant mass loadings ($<50\ \mu g\ m^{-3}$), most similar to the median yield group (AMT1) at median mass loadings ($50-110\ \mu g\ m^{-3}$) and closest to highest yield group (AO) at the highest mass loadings ($>110\ \mu g\ m^{-3}$). Using a single curve (Section 3.1) to describe all experiments increases the MSRE to 24.64×10^{-2}.

3.4. Influence of Isomers on SOA Elemental Ratio.

While a general O/R and H/R is observed for the 17 aromatic precursors studied, some minor variations are observed between isomers (Figure 4; Figure S2). SOA formed from *m*-xylene and 1,3,5-trimethylbenzene show slightly higher H/R and lower O/R compared with their aromatic isomers, which indicates a slightly lower overall oxidation of the meta isomers compared to the ortho and para isomers. However, there is no significant H/R and O/R difference among meta, para, and ortho ethyltoluenes due to the effect of a longer chain alkyl substitute attached to aromatic ring.[46] Propylbenzene and isopropylbenzene photooxidation have somewhat lower H/R and higher O/R than the other C_9 isomer suggesting that the longer alkyl substitutes may themselves partially oxidize.

4. DISCUSSION

There are ongoing initiatives to identify and account for all possible processes related to SOA formation from hydrocarbon precursors. Advanced models are being developed as more mechanisms are clarified, while the gap between model prediction and measured data continues to suggest that further work is needed. However, there remains a need to simplify these processes in order to reasonably estimate aerosol formation in atmospheric models, while using a practical number of environmental chamber experiments and computing modules. The two-product model is extensively used in current atmospheric models[10,47−49] and extends to various models[17−21] as a result of its simplicity. A modified two-product model has been developed in this work to upgrade the model predictions without increasing fitting parameters.

While precursor carbon number is expected to influence SOA formation, increasing one alkyl carbon number only decreases the vapor pressure 0.3 times,[50] a comparatively small
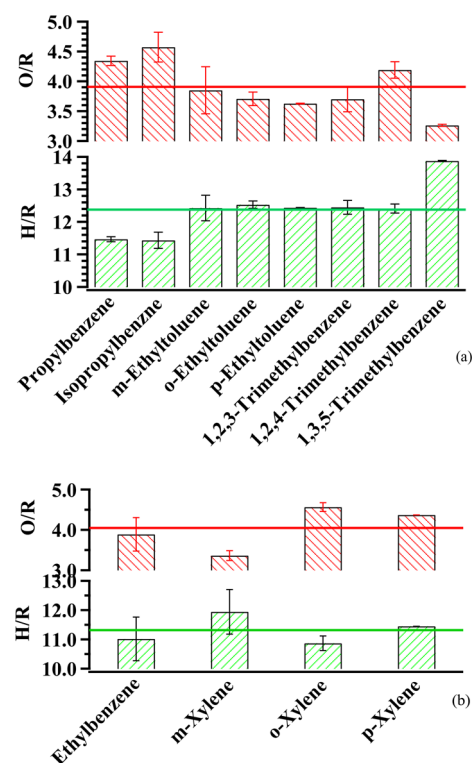

Figure 4. Aromatic ring-based elemental ratios from photooxidation of C_9 (a) and C_8 (b) aromatic hydrocarbons. Error bars are H/R and O/R standard deviation of all experiments in the photooxidation of each aromatic hydrocarbon. Red lines are average O/R values for C_8 and C_9 isomers. Green dashed lines are average H/R values for C_8 and C_9 isomers.

change compared with reactions such as functionalization. SOA yield increases with the carbon number agree with the precursor vapor pressure decrease trend for *n*-alkanes.[51] However, studies on aromatic precursors observe decreases in SOA yield with increasing precursor carbon number.[26,28,29,33,39] This indicates mechanisms more than functionalization contribute to the photooxidation of aromatic hydrocarbons since lower vapor pressure aromatic precursor produces less low volatility products on a mass basis. The matter of fact is that VOC oxidation is a combination of functionalization, fragmentation, and oligomerization.[52,53] The ring-normalized SOA yield analyzes SOA yield data on a mole basis or functional group (aromatic ring) basis of SOA precursors, instead of mass basis. This adjustment provides further insights into SOA formation mechanism by directly using SOA yield. The current study demonstrates that ring-normalized SOA yields (Yield′) are similar among all aromatic hydrocarbons. It indicates that the aromatic ring structure is a driving force for SOA formation during aromatic hydrocarbon photooxidation. Alkyl substitute impacts on aromatic hydrocarbon reaction rate and reaction mechanism are less prominent compared with aromatic ring structure. The valuable contribution of the ring-normalized yield to SOA model prediction is that SOA yield for aromatic hydrocarbon can be simply represented by a single set of parameters (α and K_{om}) instead of relying on various sets of parameters specifically for individual precursors.

Previous studies identified similar aromatic oxidation products from various aromatic precursors.[54,55] It is likely that most aromatics have similar reaction pathways with branching ratios determined by oxidation conditions and

molecular structure. Earlier work demonstrated that the reaction activities ($k_{OH}*[OH]$) are comparable during the photooxidation of all 17 aromatic precursors studied.[33,46] The current work found a similar amount of oxygen added per aromatic precursor ring for all 17 aromatic hydrocarbons studied. The O/R standard deviation is only 6.4% of its average value, while the O/C standard deviation is 27.1% of O/C average (0.48 ± 0.13). Similar O/R values and their trend are expected to observe among all the aromatic hydrocarbons under ambient conditions since a measurable evolution of H/C and O/C is not observed for aromatic precursors[33,46] as oxidation levels are changed through the course of the experiment. Additionally, the hydrogen per aromatic ring in resulting SOA is determined by the number of hydrogens in the aromatic precursor. These findings address the SOA chemical composition similarity found in aromatic hydrocarbon oxidation, which is consistent with the similar ring-normalized adjusted yield (Yield′). The similarities can only be observed when SOA yield and chemical composition are analyzed on an aromatic ring basis developed in this work. These aromatic hydrocarbons are different in alkyl substitute number and structure with only the aromatic ring as the common structure for all the aromatic hydrocarbons. This work demonstrates that the aromatic ring, not the alkyl substitutes, is the key contributor to the SOA formation from aromatic hydrocarbons. SOA formation from bicyclic hydroperoxides pathway[56] and oligomerization[33] maintains the alkyl substitutes in the oxidation products and relies on the aromatic ring to the form the oxidized products. Therefore, bicyclic hydroperoxides pathway and oligomerization are suggested as two potential mechanisms leading to the similarity in SOA formation from different aromatics observed in this work. The success of applying a ring-based chemical composition analysis in aromatic hydrocarbon studies indicates the importance of a molecular structure (aromatic ring)-based chemical composition analysis, which could possibly extended to other groups of SOA precursors.

SOA yield and composition trends discussed in this work are all based on aromatic photooxidation under NO_x conditions simulating urban area. This work provides more realistic SOA yield of aromatics under ambient conditions than earlier works (e.g., Odum et al.[13]). More important, this work provides a single curve prediction method for SOA yield of aromatics, which is even simpler than the two yield groups suggested by Odum et al.[13] The current work demonstrates that the oxidation of the aromatic hydrocarbon ring and not of the alkyl substituents is the driving force for SOA formation and composition from single ring aromatic hydrocarbons. This ring-normalized SOA yield method is initially applied to an existing aromatic hydrocarbon photooxidation data set; however, its use need not be necessarily restricted to aromatics and should be evaluated on other classes of SOA precursors. The core of the concept is to compare SOA formation from a group of similar precursors on a basis of the critical functional group. Application of this method in future studies may facilitate understanding of SOA formation mechanism.

■ ASSOCIATED CONTENT

Ⓢ Supporting Information

The Supporting Information is available free of charge on the ACS Publications website at DOI: 10.1021/acs.est.5b05778.

Mean squared relative error (MSRE) for each two-product model fittings of Yield′ and M_0. Traditional mass-based SOA yield as a function of M_0 for 17 aromatic hydrocarbons. H/R and O/R variation for SOA from different C_8 and C_9 aromatic isomers. (PDF)

■ AUTHOR INFORMATION

Corresponding Author

*Tel: +1 951 781 5695. Fax: +1 951 781 5790. E-mail: dcocker@engr.ucr.edu.

Present Address

S. Nakao is currently at the Department of Chemical and Biomolecular Engineering, Clarkson University, Potsdam, New York 13699, United States.

Notes

The authors declare no competing financial interest.

■ REFERENCES

(1) Volkamer, R.; Jimenez, J. L.; San Martini, F.; Dzepina, K.; Zhang, Q.; Salcedo, D.; Molina, L. T.; Worsnop, D. R.; Molina, M. J. Secondary organic aerosol formation from anthropogenic air pollution: Rapid and higher than expected. *Geophys. Res. Lett.* **2006**, *33* (17), L17811.

(2) Gaydos, T. M.; Pinder, R.; Koo, B.; Fahey, K. M.; Yarwood, G.; Pandis, S. N. Development and application of a three-dimensional aerosol chemical transport model, PMCAMx. *Atmos. Environ.* **2007**, *41* (12), 2594−2611.

(3) Henze, D. K.; Seinfeld, J. H.; Ng, N. L.; Kroll, J. H.; Fu, T.-M.; Jacob, D. J.; Heald, C. L. Global modeling of secondary organic aerosol formation from aromatic hydrocarbons: high-vs. low-yield pathways. *Atmos. Chem. Phys.* **2008**, *8* (9), 2405−2421.

(4) Matsui, H.; Koike, M.; Takegawa, N.; Kondo, Y.; Griffin, R. J.; Miyazaki, Y.; Yokouchi, Y.; Ohara, T. Secondary organic aerosol formation in urban air: Temporal variations and possible contributions from unidentified hydrocarbons. *J. Geophys. Res.* **2009**, *114* (D4), D04201.

(5) Hallquist, M.; Wenger, J. C.; Baltensperger, U.; Rudich, Y.; Simpson, D.; Claeys, M.; Dommen, J.; Donahue, N. M.; George, C.; Goldstein, A. H.; Hamilton, J. F.; Herrmann, H.; Hoffmann, T.; Iinuma, Y.; Jang, M.; Jenkin, M. E.; Jimenez, J. L.; Kiendler-Scharr, A.; Maenhaut, W.; McFiggans, G.; Mentel, Th. F.; Monod, A.; Prévôt, A. S. H.; Seinfeld, J. H.; Surratt, J. D.; Szmigielski, R.; Wildt, J. The formation, properties and impact of secondary organic aerosol: current and emerging issues. *Atmos. Chem. Phys.* **2009**, *9* (14), 5155−5236.

(6) Farina, S. C.; Adams, P. J.; Pandis, S. N. Modeling global secondary organic aerosol formation and processing with the volatility basis set: Implications for anthropogenic secondary organic aerosol. *J. Geophys. Res.* **2010**, *115* (D9), D09202.

(7) Hayes, P. L.; Carlton, A. G.; Baker, K. R.; Ahmadov, R.; Washenfelder, R. A.; Alvarez, S.; Rappenglück, B.; Gilman, J. B.; Kuster, W. C.; de Gouw, J. A.; Zotter, P.; Prévôt, A. S. H.; Szidat, S.; Kleindienst, T. E.; Offenberg, J. H.; Ma, P. K.; Jimenez, J. L. Modeling the formation and aging of secondary organic aerosols in Los Angeles during CalNex 2010. *Atmos. Chem. Phys.* **2015**, *15* (10), 5773−5801.

(8) Tsimpidi, A. P.; Karydis, V. A.; Zavala, M.; Lei, W.; Molina, L.; Ulbrich, I. M.; Jimenez, J. L.; Pandis, S. N. Evaluation of the volatility basis-set approach for the simulation of organic aerosol formation in

the Mexico City metropolitan area. *Atmos. Chem. Phys.* **2010**, *10* (2), 525−546.

(9) Woody, M. C.; Baker, K. R.; Hayes, P. L.; Jimenez, J. L.; Koo, B.; Pye, H. O. Understanding sources of organic aerosol during CalNex-2010 using the CMAQ-VBS. *Atmos. Chem. Phys.* **2016**, *16* (6), 4081−4100.

(10) Kanakidou, M.; Seinfeld, J. H.; Pandis, S. N.; Barnes, I.; Dentener, F. J.; Facchini, M. C.; Van Dingenen, R.; Ervens, B.; Nenes, A.; Nielsen, C. J.; Swietlicki, E.; Putaud, J. P.; Balkanski, Y.; Fuzzi, S.; Horth, J.; Moortgat, G. K.; Winterhalter, R.; Myhre, C. E. L.; Tsigaridis, K.; Vignati, E.; Stephanou, E. G.; Wilson, J. Organic aerosol and global climate modelling: a review. *Atmos. Chem. Phys.* **2005**, *5* (4), 1053−1123.

(11) Derwent, R. G.; Jenkin, M. E.; Utembe, S. R.; Shallcross, D. E.; Murrells, T. P.; Passant, N. R. Secondary organic aerosol formation from a large number of reactive man-made organic compounds. *Sci. Total Environ.* **2010**, *408* (16), 3374−3381.

(12) Freney, E. J.; Sellegri, K.; Canonaco, F.; Colomb, A.; Borbon, A.; Michoud, V.; Doussin, J.-F.; Crumeyrolle, S.; Amarouche, N.; Pichon, J.-M.; Bourianne, T.; Gomes, L.; Prevot, A. S. H.; Beekmann, M.; Schwarzenböeck, A. Characterizing the impact of urban emissions on regional aerosol particles: airborne measurements during the MEGAPOLI experiment. *Atmos. Chem. Phys.* **2014**, *14* (3), 1397−1412.

(13) Odum, J. R.; Hoffmann, T.; Bowman, F.; Collins, D.; Flagan, R. C.; Seinfeld, J. H. Gas/particle partitioning and secondary organic aerosol yields. *Environ. Sci. Technol.* **1996**, *30* (8), 2580−2585.

(14) Lim, Y. B.; Tan, Y.; Perri, M. J.; Seitzinger, S. P.; Turpin, B. J. Aqueous chemistry and its role in secondary organic aerosol (SOA) formation. *Atmos. Chem. Phys.* **2010**, *10*, 10521−10539.

(15) Jang, M.; Czoschke, N. M.; Lee, S.; Kamens, R. M. Heterogeneous atmospheric aerosol production by acid-catalyzed particle-phase reactions. *Science* **2002**, *298* (5594), 814−817.

(16) Pankow, J. F. An absorption model of gas/particle partitioning of organic compounds in the atmosphere. *Atmos. Environ.* **1994**, *28* (2), 185−188.

(17) Donahue, N. M.; Robinson, A. L.; Stanier, C. O.; Pandis, S. N. Coupled partitioning, dilution, and chemical aging of semivolatile organics. *Environ. Sci. Technol.* **2006**, *40* (8), 2635−2643.

(18) Pankow, J. F.; Barsanti, K. C. The carbon number-polarity grid: A means to manage the complexity of the mix of organic compounds when modeling atmospheric organic particulate matter. *Atmos. Environ.* **2009**, *43* (17), 2829−2835.

(19) Barsanti, K. C.; Smith, J. N.; Pankow, J. F. Application of the np+mP modeling approach for simulating secondary organic particulate matter formation from α-pinene oxidation. *Atmos. Environ.* **2011**, *45* (37), 6812−6819.

(20) Donahue, N. M.; Kroll, J.; Pandis, S. N.; Robinson, A. L. A two-dimensional volatility basis set−Part 2: Diagnostics of organic-aerosol evolution. *Atmos. Chem. Phys.* **2012**, *12* (2), 615−634.

(21) Cappa, C. D.; Wilson, K. R. Multi-generation gas-phase oxidation, equilibrium partitioning, and the formation and evolution of secondary organic aerosol. *Atmos. Chem. Phys.* **2012**, *12* (20), 9505−9528.

(22) Aumont, B.; Szopa, S.; Madronich, S. Modelling the evolution of organic carbon during its gas-phase tropospheric oxidation: development of an explicit model based on a self generating approach. *Atmos. Chem. Phys.* **2005**, *5* (9), 2497−2517.

(23) Valorso, R.; Aumont, B.; Camredon, M.; Raventos-Duran, T.; Mouchel-Vallon, C.; Ng, N. L.; Seinfeld, J. H.; Lee-Taylor, J.; Madronich, S. Explicit modelling of SOA formation from α-pinene photooxidation: sensitivity to vapour pressure estimation. *Atmos. Chem. Phys.* **2011**, *11* (14), 6895−6910.

(24) Zhang, X.; Seinfeld, J. H. A functional group oxidation model (FGOM) for SOA formation and aging. *Atmos. Chem. Phys.* **2013**, *13* (12), 5907−5926.

(25) Zuend, A.; Marcolli, C.; Peter, T.; Seinfeld, J. H. Computation of liquid-liquid equilibria and phase stabilities: implications for RH-dependent gas/particle partitioning of organic-inorganic aerosols. *Atmos. Chem. Phys.* **2010**, *10* (16), 7795−7820.

(26) Shiraiwa, M.; Pfrang, C.; Koop, T.; Pöschl, U. Kinetic multi-layer model of gas-particle interactions in aerosols and clouds (KM-GAP): linking condensation, evaporation and chemical reactions of organics, oxidants and water. *Atmos. Chem. Phys.* **2012**, *12* (5), 2777−2794.

(27) Jathar, S. H.; Cappa, C. D.; Wexler, A. S.; Seinfeld, J. H.; Kleeman, M. J. Multi-generational oxidation model to simulate secondary organic aerosol in a 3-D air quality model. *Geosci. Model. Dev. Discuss.* **2015**, *8* (2), 1857−1891.

(28) Odum, J. R.; Jungkamp, T.; Griffin, R.; Flagan, R. C.; Seinfeld, J. H. The atmospheric aerosol-forming potential of whole gasoline vapor. *Science* **1997**, *276* (5309), 96−99.

(29) Cocker, D. R., III; Mader, B. T.; Kalberer, M.; Flagan, R. C.; Seinfeld, J. H. The effect of water on gas−particle partitioning of secondary organic aerosol: II. *m*-xylene and 1, 3, 5-trimethylbenzene photooxidation systems. *Atmos. Environ.* **2001**, *35* (35), 6073−6085.

(30) Song, C.; Na, K.; Cocker, D. R., III Impact of the hydrocarbon to NO$_x$ ratio on secondary organic aerosol formation. *Environ. Sci. Technol.* **2005**, *39* (9), 3143−3149.

(31) Song, C.; Na, K.; Warren, B.; Malloy, Q.; Cocker, D. R., III Secondary organic aerosol formation from the photooxidation of *p*-and *o*-xylene. *Environ. Sci. Technol.* **2007**, *41* (21), 7403−7408.

(32) Ng, N. L.; Kroll, J. H.; Chan, A. W. H.; Chhabra, P. S.; Flagan, R. C.; Seinfeld, J. H. Secondary organic aerosol formation from m-xylene, toluene, and benzene. *Atmos. Chem. Phys.* **2007**, *7* (14), 3909−3922.

(33) Li, L.; Tang, P.; Nakao, S.; Chen, C.-L.; Cocker, R. D., III Role of methyl group number on SOA formation from aromatic hydrocarbons photooxidation under low NO$_x$ conditions. *Atmos. Chem. Phys.* **2016**, *16*, 2255−2272.

(34) Aiken, A. C.; DeCarlo, P. F.; Jimenez, J. L. Elemental analysis of organic species with electron ionization high-resolution mass spectrometry. *Anal. Chem.* **2007**, *79* (21), 8350−8358.

(35) Aiken, A. C.; DeCarlo, P. F.; Kroll, J. H.; Worsnop, D. R.; Huffman, J. A.; Docherty, K. S.; Ulbrich, I. M.; Mohr, C.; Kimmel, J. R.; Sueper, D.; et al. O/C and OM/OC ratios of primary, secondary, and ambient organic aerosols with high-resolution time-of-flight aerosol mass spectrometry. *Environ. Sci. Technol.* **2008**, *42* (12), 4478−4485.

(36) Heald, C. L.; Kroll, J. H.; Jimenez, J. L.; Docherty, K. S.; DeCarlo, P. F.; Aiken, A. C.; Chen, Q.; Martin, S. T.; Farmer, D. K.; Artaxo, P. A simplified description of the evolution of organic aerosol composition in the atmosphere. *Geophys. Res. Lett.* **2010**, *37*, L08803.

(37) Chhabra, P. S.; Ng, N. L.; Canagaratna, M. R.; Corrigan, A. L.; Russell, L. M.; Worsnop, D. R.; Flagan, R. C.; Seinfeld, J. H. Elemental composition and oxidation of chamber organic aerosol. *Atmos. Chem. Phys.* **2011**, *11* (17), 8827−8845.

(38) Loza, C. L.; Chhabra, P. S.; Yee, L. D.; Craven, J. S.; Flagan, R. C.; Seinfeld, J. H. Chemical aging of *m*-xylene secondary organic aerosol: laboratory chamber study. *Atmos. Chem. Phys.* **2012**, *12* (1), 151−167.

(39) Sato, K.; Takami, A.; Kato, Y.; Seta, T.; Fujitani, Y.; Hikida, T.; Shimono, A.; Imamura, T. AMS and LC/MS analyses of SOA from the photooxidation of benzene and 1, 3, 5-trimethylbenzene in the presence of NO$_x$: effects of chemical structure on SOA aging. *Atmos. Chem. Phys.* **2012**, *12*, 4667−4682.

(40) Kroll, J. H.; Donahue, N. M.; Jimenez, J. L.; Kessler, S. H.; Canagaratna, M. R.; Wilson, K. R.; Altieri, K. E.; Mazzoleni, L. R.; Wozniak, A. S.; Bluhm, H.; et al. Carbon oxidation state as a metric for describing the chemistry of atmospheric organic aerosol. *Nat. Chem.* **2011**, *3* (2), 133−139.

(41) Carter, W. P.; Cocker, D. R., III; Fitz, D. R.; Malkina, I. L.; Bumiller, K.; Sauer, C. G.; Pisano, J. T.; Bufalino, C.; Song, C. A new environmental chamber for evaluation of gas-phase chemical mechanisms and secondary aerosol formation. *Atmos. Environ.* **2005**, *39* (40), 7768−7788.

(42) Cocker, D. R., III; Flagan, R. C.; Seinfeld, J. H. State-of-the art chamber facility for studying atmospheric aerosol chemistry. *Environ. Sci. Technol.* **2001**, *35*, 2594−2601.

(43) Malloy, Q. G.; Nakao, S.; Qi, L.; Austin, R.; Stothers, C.; Hagino, H.; Cocker, D. R., III Real-Time Aerosol Density Determination Utilizing a Modified Scanning Mobility Particle Sizer − Aerosol Particle Mass Analyzer System. *Aerosol Sci. Technol.* **2009**, *43*, 673−678.

(44) Canagaratna, M. R.; Jayne, J. T.; Jimenez, J. L.; Allan, J. D.; Alfarra, M. R.; Zhang, Q.; Onasch, T. B.; Drewnick, F.; Coe, H.; Middlebrook, A.; Delia, A.; Williams, L. R.; Trimborn, A. M.; Northway, M. J.; DeCarlo, P. F.; Kolb, C. E.; Davidovits, P.; Worsnop, D. R. Chemical and microphysical characterization of ambient aerosols with the aerodyne aerosol mass spectrometer. *Mass Spectrom. Rev.* **2007**, *26*, 185−222.

(45) DeCarlo, P. F.; Kimmel, J. R.; Trimborn, A.; Northway, M. J.; Jayne, J. T.; Aiken, A. C.; Gonin, M.; Fuhrer, K.; Horvath, T.; Docherty, K. S.; Worsnop, D. R.; Jimenez, J. L Field-deployable, high-resolution, time-of-flight aerosol mass spectrometer. *Anal. Chem.* **2006**, *78*, 8281−8289.

(46) Li, L.; Tang, P.; Nakao, S.; Cocker, R. D., III Impact of molecular structure on secondary organic aerosol formation from aromatic hydrocarbon photooxidation under low NO$_x$ conditions. *Atmos. Chem. Phys. Discuss.* **2016**, *15*, 1−40.

(47) Binkowski, F. S.; Roselle, S. J. Models-3 Community Multiscale Air Quality (CMAQ) model aerosol component 1. Model description. *J. Geophys. Res.* **2003**, *108* (D6), 4183.

(48) Jenkin, M.; Saunders, S.; Wagner, V.; Pilling, M. Protocol for the development of the Master Chemical Mechanism, MCM v3 (Part B): tropospheric degradation of aromatic volatile organic compounds. *Atmos. Chem. Phys.* **2003**, *3* (1), 181−193.

(49) Tsigaridis, K.; Kanakidou, M. Global modelling of secondary organic aerosol in the troposphere: a sensitivity analysis. *Atmos. Chem. Phys.* **2003**, *3* (5), 1849−1869.

(50) Pankow, J. F.; Asher, W. E. SIMPOL. 1: a simple group contribution method for predicting vapor pressures and enthalpies of vaporization of multifunctional organic compounds. *Atmos. Chem. Phys.* **2008**, *8* (10), 2773−2796.

(51) Lim, Y. B.; Ziemann, P. J. Products and mechanism of secondary organic aerosol formation from reactions of n-alkanes with OH radicals in the presence of NO$_x$. *Environ. Sci. Technol.* **2005**, *39* (23), 9229−9236.

(52) Jimenez, J. L.; Canagaratna, M. R.; Donahue, N. M.; Prevot, A. S. H.; Zhang, Q.; Kroll, J. H.; DeCarlo, P. F.; Allan, J. D.; Coe, H.; Ng, N. L.; Aiken, A. C.; Docherty, K. S.; Ulbrich, I. M.; Grieshop, A. P.; Robinson, A. L.; Duplissy, J.; Smith, J. D.; Wilson, K. R.; Lanz, V. A.; Hueglin, C.; Sun, Y. L.; Tian, J.; Laaksonen, A.; Raatikainen, T.; Rautiainen, J.; Vaattovaara, P.; Ehn, M.; Kulmala, M.; Tomlinson, J. M.; Collins, D. R.; Cubison, M. J.; Dunlea, E. J.; Huffman, J. A.; Onasch, T. B.; Alfarra, M. R.; Williams, P. I.; Bower, K.; Kondo, Y.; Schneider, J.; Drewnick, F.; Borrmann, S.; Weimer, S.; Demerjian, K.; Salcedo, D.; Cottrell, L.; Griffin, R.; Takami, A.; Miyoshi, T.; Hatakeyama, S.; Shimono, A.; Sun, J. Y.; Zhang, Y. M.; Dzepina, K.; Kimmel, J. R.; Sueper, D.; Jayne, J. T.; Herndon, S. C.; Trimborn, A. M.; Williams, L. R.; Wood, E. C.; Middlebrook, A. M.; Kolb, C. E.; Baltensperger, U.; Worsnop, D. R. Evolution of organic aerosols in the atmosphere. *Science* **2009**, *326* (5959), 1525−1529.

(53) Kroll, J. H.; Smith, J. D.; Che, D. L.; Kessler, S. H.; Worsnop, D. R.; Wilson, K. R. Measurement of fragmentation and functionalization pathways in the heterogeneous oxidation of oxidized organic aerosol. *Phys. Chem. Chem. Phys.* **2009**, *11* (36), 8005−8014.

(54) Forstner, H. J. L.; Flagan, R. C.; Seinfeld, J. H. Secondary organic aerosol from the photooxidation of aromatic hydrocarbons: Molecular composition. *Environ. Sci. Technol.* **1997**, *31* (5), 1345−1358.

(55) Kleindienst, T.; Smith, D.; Li, W.; Edney, E.; Driscoll, D.; Speer, R.; Weathers, W. Secondary organic aerosol formation from the oxidation of aromatic hydrocarbons in the presence of dry submicron ammonium sulfate aerosol. *Atmos. Environ.* **1999**, *33* (22), 3669−3681.

(56) Carter, W. P. L.; Heo, G. Development of revised SAPRC aromatics mechanisms. *Atmos. Environ.* **2013**, *77*, 404−414.